Carbon 148 (2019) 267–276

Contents lists available at ScienceDirect

Carbon

journal homepage: www.elsevier.com/locate/carbon

Micro-mechanism and influencing factors of graphene foam elasticity

Chao Wang [a], Cun Zhang [b], Shaohua Chen [c, d, *]

[a] LNM, Institute of Mechanics, Chinese Academy of Sciences, Beijing, 100190, China
[b] Department of Engineering Mechanics, Shijiazhuang Tiedao University, Shijiazhuang, 050043, China
[c] Institute of Advanced Structure Technology, Beijing Institute of Technology, Beijing, 100081, China
[d] Beijing Key Laboratory of Lightweight Multi-functional Composite Materials and Structures, Beijing Institute of Technology, Beijing, 100081, China

ARTICLE INFO

Article history:
Received 14 January 2019
Received in revised form
9 March 2019
Accepted 25 March 2019
Available online 28 March 2019

Keywords:
Graphene foam
Super-elasticity
Nonuniformity
Deformation mechanism
Coarse-grained molecular dynamics

ABSTRACT

The emerging graphene foams (GrFs) have received increasing attention in both scientific and engineering fields in recent years. A good elasticity is the prerequisite for its further applications. However, the mechanism and basic characteristics of elasticity of GrFs have not been understood clearly so far. In this paper, we conduct systematic simulations of compression-uncompression and tension-untension to study the characteristics of GrF elasticity using the coarse-grained molecular dynamics (CGMD) method. We find that deformation of GrFs is highly nonuniform at the scale of both flakes and regions, which is qualitatively consistent with the experimental observations. The deformation of GrFs is dominated by the flake bending rather than stretching, which is independent of the loading type, size, shape or thickness of flakes, as well as the density or stiffness of crosslinks. The great asymmetry of elasticity under tension and compression is induced by different mode of bond breaking. Furthermore, by evaluating the elastic energy density, we find that both thicker flakes and more crosslinks are two key factors responsible for good elasticity of GrFs. These results should be useful for understanding GrF elasticity and further design of advanced graphene-based materials.

1. Introduction

Graphene foam (GrF) [1–3] is a new kind of porous bulk material composed of randomly distributed graphene flakes interconnected by weak van der Waals forces and strong chemical bonds. It features a series of excellent physical [4–6] and mechanical [1,2,4] properties due to its inheritance of advantages of both porous materials and two-dimensional (2D) graphene, which enables many potential applications in the field of sensing [5], lithium ion batteries [6], sorbent materials [7], stretchable electronics [8] and damping materials [2]. Due to the wide range of applications, graphene foam has achieved much attention in both scientific and engineering fields in recent years. Most efforts have been dedicated to developing fabrication technologies [1–3,8,9] to make graphene foams with advanced properties by tuning the morphology of microstructures. Several typical deformation behaviors as well as some mechanical and electrical properties have been identified experimentally. They exhibit a rubber-like constitutive response to uniaxial compression [1–3,10] with a tunable Poisson's ratio [1,2] in a wide range $-0.30 < \nu < 0.46$, and have a multi-peak stress-strain response to uniaxial tension [11]. They possess a strong capability of energy dissipation [1,3,4,12,13] indicated by the hysteresis loops in the stress-strain curves and have a wide-range temperature- and loading frequency-insensitive viscoelastic properties [2,14], similar to carbon nanotube networks [15]. They exhibit an excellent super-compressive elasticity [1–4,10] of 99% recovery under cyclic compression load and good conductivity [3,8,12,13] tuned precisely by strain.

In order to understand the underlying mechanism of these outstanding properties and experimental results, theoretical and mainly computational techniques are used. Baimova et al. [16] carried out full-atom molecular dynamics (MD) simulations to study the mechanical response of GrFs under shear strain and found that the shear deformation could change foams' microstructures and mechanical properties. Nieto et al. [11] experimentally observed two main multi-scale deformation mechanisms of flake bending and cell-wall elastic depression under nanoindentation and uniaxial tension by *in situ* SEM tests. Wang et al. [17] correlated the rubber-like constitutive relationship of graphene foams under uniaxial compression with microstructural

* Corresponding author. Institute of Advanced Structure Technology, Beijing Institute of Technology, Beijing, 100081, China.
E-mail addresses: chenshaohua72@hotmail.com, shchen@bit.edu.cn (S. Chen).

https://doi.org/10.1016/j.carbon.2019.03.084
0008-6223/

evolutions using CGMD method and found that the flake thickness and compressive strain are two key factors controlling Poisson's effect. Pan et al. [18] further found that the macroscopic multi-peak stress-strain relationship is induced by the microscopic intermittent bond-breaking of flakes and crosslinks, and a mechanical interlocking mechanism among hole-flakes [19] in the uniaxial compression and recovery behaviors of hole-flake graphene foams. Nautiyal et al. [20] and Wang et al. [21] investigated the energy dissipation mechanism of GrFs and uncovered the key dissipative mechanism of flake sliding, impacting and rippling using the localized nanoscale dynamics mechanical testing and CGMD simulation, respectively. With experimental method of free casting and thermal reduction, and another coarse-grained (CG) model [24], Ni et al. [22] and Shen et al. [23] respectively found that the size of graphene flakes plays an important role in both structural and mechanical properties of GrFs. Xia et al. [25] studied the dynamics of GrFs using the same CG model [24] and found bulk foam materials have an exceptionally large free-volume and high thermal stability due to their high glass-transition temperature as compared to conventional polymer materials. Liu et al. [26] carried out the first theoretical study of electrical conductivity of 3D GrFs combining with transport modeling and CGMD simulations, and successfully explained the phenomenon of the maximum and strain-tunable properties of electrical conductivity. Qin et al. [27] found the scaling law of the compressive and tensile strength as a function of density of 3D GrFs with different power indexes of 3.01 and 2.01 using full-atom MD simulations.

As a basic scaffold of new materials and devices, the elasticity of GrFs is mainly responsible for the structural skeleton integrity under loads, a key indicator in all applications. Although GrFs with extraordinary compressive elasticity have been synthesized and highlighted in many works [1–4,10], the underlying mechanisms given are still diverse, qualitative and speculative. For example, Xu et al. [1] qualitatively attributed the super-compressive elasticity to the special core-shell-like frameworks and thick cell walls of foams based on the SEM/TEM microstructure analysis; Wu et al. [2] speculated that the functional group plays a central role in covalently interconnect graphene flakes to form a monolithic 3D foam networks with super compressive elasticity, but could not provide any direct experimental or simulation evidence of chemical group effects. This is attributed to the complex deformation behaviors and properties of graphene foams, which are influenced by many factors at both atomic and flake scales, including geometrical characteristics and deformation modes of ingredient flakes, parameters of inter-flake crosslinks, and microstructural evolutions. It is of great difficulties and almost impossible to accurately tune and monitor these factors by existing experimental techniques. As a result, so far, it is still elusive what the key factors are and how they dominate the compressive elasticity of graphene foams? Furthermore, during service, GrFs are not only compressed but may also be stretched, or even subjected to more complex loads. A good tensile elasticity should be of equal importance for graphene foams. However, in sharp contrast to the outstanding super-compressive elasticity, graphene foams have a poor tensile performance with a small fracture strain of less than 10% as observed by Wu et al. [2] and Nieto et al. [11]. The tensile elasticity of graphene foams has not been studied till now. Therefore, what is the elastic behavior of graphene foams under tension and what are the common characteristics or major differences between the tensile elasticity and the compressive one?

A comprehensive investigation on the elastic mechanism of GrFs from the scale of constituent flake to system is desperately needed to clarify these basic and essential issues. This should be very useful for the design of advanced graphene foams as scaffolds of materials and devices in real applications. In addition to this point, with the flourish development of 2D materials in recent years, such as graphene-oxide, molybdenum disulfide (MoS_2), hexagonal boron nitride (hBN), *etc.* [28], more kinds of foam materials are needed to be assembled by these emerging 2D building blocks to achieve targeted macroscopic properties. This study should also be useful for understanding the elasticity of related nano-porous materials.

In this paper, the 2D mesoscopic graphene model [29] is used to construct a 3D model of GrFs to study the elastic mechanism of such a new kind of porous material. The mechanical behavior of graphene foams under uniaxial compression and tension has been successfully implemented in our previous works [17,18], and a series of mechanical and physical phenomena of the Poisson's effect, energy dissipation and electrical conductivity have been well explained as mentioned above. The rest of this paper is organized as follows. First, the numerical model of graphene foam is introduced, based on which the elastic property of GrFs under both uniaxial tension and compression is reproduced numerically. Three basic characteristics of elastic deformation non-uniformity at the scale of flake, the flake-bending-dominated elastic deformation and the tension-compression asymmetry are carefully analyzed, respectively. The effect of the flake size, thickness, crosslink density and stiffness on the storage of elastic energy is studied in detail. Conclusions are given at the end of this paper.

2. 2D mesoscopic graphene model and 3D numerical GrF sample

Based on the equivalent energy principle and systematic full-atom MD calculations of a mechanical test suite, a 2D CG mesoscopic model for a graphene flake was established by Cranford and Buehler [29], which had already been proved to characterize the tensile, shear deformation as well as the bending of a graphene sheet and even more complicated deformation of twist and coil. In the 2D mesoscopic model, each coarse grain represents an atomically single- or multilayer graphene sheet with an area $2.5 \times 2.5\,nm^2$. A harmonic spring potential $\phi_T = k_T(r-r_0)^2/2$ is used to describe the axial stretching energy among all pairs of bonded CG particles, where k_T denotes a spring constant and r is the distance between neighboring particles with an equilibrium distance $r_0 = 2.5\,nm$. A harmonic rotational-spring potential $\phi_\varphi = k_\varphi(\varphi-\varphi_0)^2/2$ is used to describe the in-plane bending energy under shear deformation, where k_φ denotes the spring constant related to the bending angle φ among three particles with a referenced equilibrium angle of $\varphi_0 = 90°$. $\phi_\theta = k_\theta(\theta\text{-}\theta_0)^2/2$ denotes the out-of-plane bending energy with a spring constant k_θ, where θ denotes the bending angle among three particles with a referenced equilibrium value of $\theta_0 = 180°$. The weak van der Waals interaction between neighboring CG flakes is described using the Lennard-Jones (LJ) potential $\phi_{LJ} = 4\varepsilon[(\sigma/r)^{12}\text{-}(\sigma/r)^6]$, where ε is a parameter determining the depth of the potential well, σ is a length scale parameter that determines the position of the minimum potential, and r is the bead-to-bead distance between different flakes. As a building block, the side length of each square CG flake is 75 nm, which contains 900 beads as shown in Fig. 1b. As for the preprocessing of a graphene foam system, 100 flakes are placed randomly in a big cubic box to ensure no interaction among them. Then, NPT ensemble technique is adopted to make the system shrink with a periodic boundary condition in three directions as well as a constant temperature 300 K and one barometric pressure. A time step of 1 fs is adopted. The system was relaxed for 10 ns to reach an equilibrium state. The final configuration is shown in Fig. 1c, in which flakes are randomly oriented. One flake in real materials may contain 1-10 graphene layers [8,11,30], here, a moderate 5-layered flake is mainly adopted and the effect of thickness on elasticity is also evaluated in the paper. The

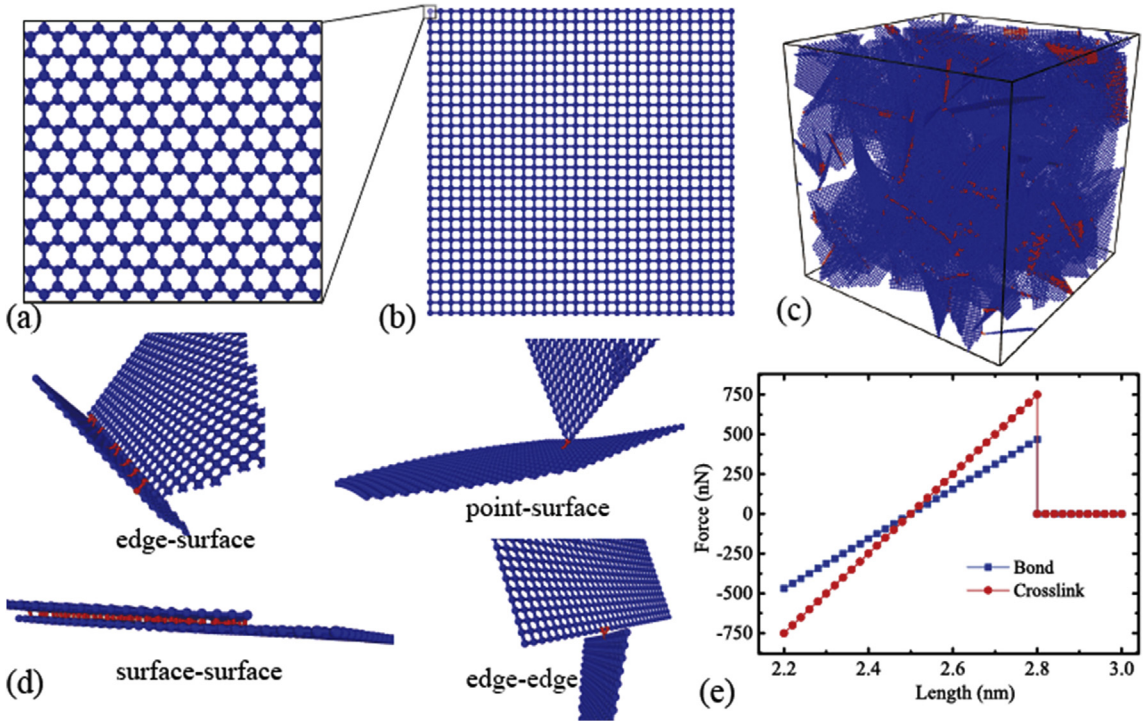

Fig. 1. (a) A square full-atomic graphene sheet with a side length of 2.5 nm; (b) The CG model of a graphene flake with a side length of 75 nm; (c) The CG model of graphene foam with crosslinks between neighboring flakes, where the crosslink is labeled in red. (d) Crosslinks (red) in four typical configurations: the edge-surface, point-surface, surface-surface and edge-edge; (e) Force-length relationships for the C-C bond in CG flakes and the crosslink between neighboring flakes. (A colour version of this figure can be viewed online.)

corresponding CG parameters of 5-layered graphene flake shown in Table 1 are fitted using the values of 1, 2, 4 and 8-layered cases given in Ref. [29]. For simplicity, all flakes in our simulations are assumed to be identical. The size of constituent graphene flakes in experiments varies from several nanometers [27] to micrometers [2], and the resulting equilibrium density of GrFs in a series of experimental studies [2,8,30] is in the range of 1–100 mg/cm^3. We have found that the equilibrium density of GrFs decreases with an increasing flake size in our previous work [17]. Considering the huge computational costs when larger CG flakes are adopted, a relatively small flake with a side length of 75 nm is used in most of our MD calculations and the corresponding equilibrium density of system is ~200 mg/cm^3.

Crosslinks are added at the edge-surface, surface-surface, edge-edge and point-surface contact regions between neighboring flakes as shown in Fig. 1d. The distribution of crosslinks in the system is non-uniform due to the irregularity of foam system. A harmonic spring potential $\phi_c = k_c(l-l_0)^2/2$ is used to describe the stretching energy of crosslinks, where k_c denotes a spring constant and l is the current length of crosslinks. $l_0 = r_0$ and $k_c = k_T$ are set in simulations if not stated specifically. The critical length of crosslinks l_c is set to be 2.8 nm, with which the fracture strain of crosslinks is about 12%, reasonably comparable with the fracture strain 12%–28% of a graphene flake given in Refs. [29,31]. The density of the number of crosslinks, i.e., the number of crosslinks per graphene flake, can be tuned flexibly in a wide range from zero to a larger value 27.5 to study the effect of link strength between flakes.

3. Results and discussion

3.1. Stress-strain relationship

In order to evaluate the characteristics of GrF elasticity, we conduct both uniaxial compression-uncompression and tension-untension simulations using the GrF numerical model in Fig. 1c to examine two related processes: the elastic energy storage process under tensile or compressive loads and the subsequent recovery process of foam structures. The simulation settings for the uncompression and untension processes are the same as those for the compression and tension processes with the thermostat (300 K), barostat in the y and z directions (zero barometric pressure) and the time step 1 fs, except that the barostat in the loading direction is resumed in the uncompression or untension process to mimic the pressure boundary condition of the foam system. First of all, the sample is uniaxially compressed or tensioned to a moderate strain 0.66 and then released to recover freely for enough time until its size is no longer changed. As shown in Fig. 2a, the absolute value of the loading strain ε_x under both compression and tension increases to a strain magnitude 0.66 and then decreases sharply along with the collapsed time and finally converges to two different residual strains 0.04 and 0.09, respectively. The constitutive relationships between the stress σ_x and strain ε_x for the two kinds of loading-unloading processes are shown in Fig. 2b, and the corresponding visual snapshots at loading strains 0, ±0.33 and ± 0.66 are shown in Fig. 2c–g and h-k. Under compression, the stress-strain

Table 1
The force field parameters for the CG model.

Parameters	k_T	r_0	k_φ	φ_0	k_θ	θ_0	σ	ε
Value	2325	25	84350	90°	140156	180°	23.84	473
Units	kcalmol^{-1}Å^{-2}	Å	kcalmol^{-1}rad^{-2}	–	kcalmol^{-1}rad^{-2}	–	Å	kcalmol^{-1}

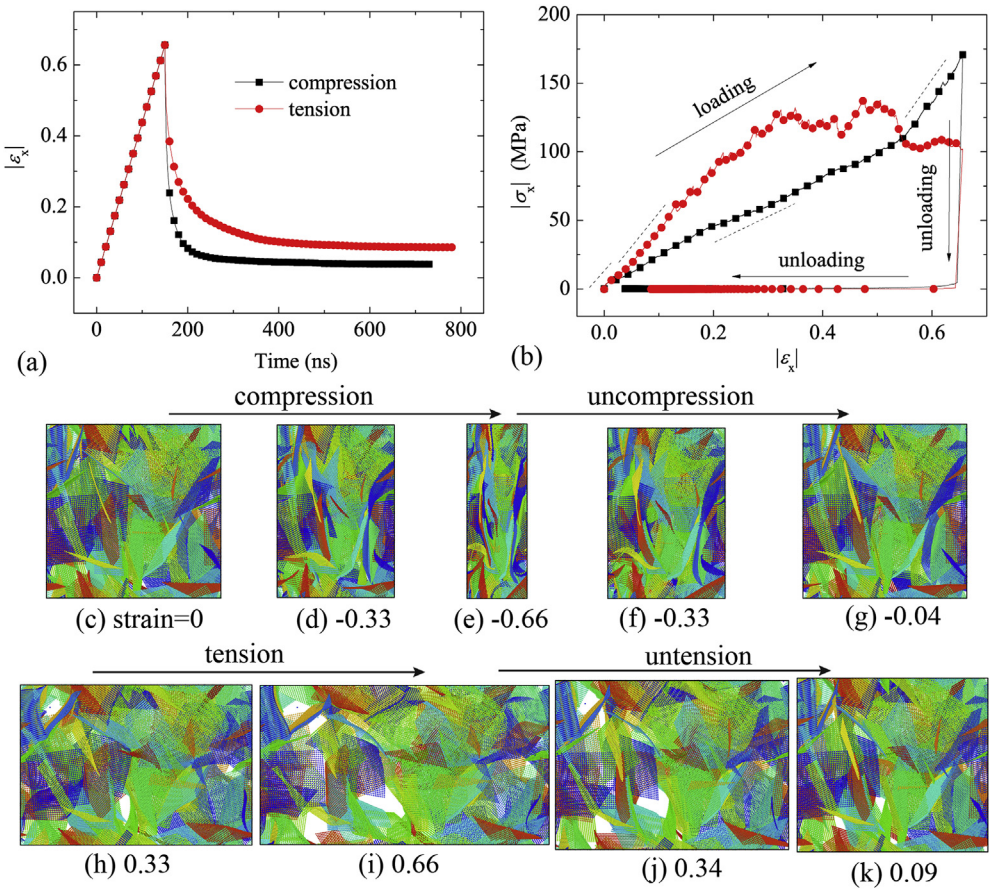

Fig. 2. (a) The strain of foam system as a function of the collapsed time in the uniaxial compression-uncompression and tension-untension processes; (b) The corresponding stress-strain relationship in two kinds of loading-unloading processes; (c-g, h-k) Snapshots in the compression-uncompression and tension-untension processes, respectively. Flakes in GrFs are labeled in different colors. (A colour version of this figure can be viewed online.)

relationship exhibits a typical three-stage characteristic with a finite stiffness in the middle stage, consistent well with that observed in experiments [3]. This is attributed to the strong chemical crosslinks between neighboring flakes as shown in Fig. 1c and d, which impose strong restrictions against flake rearrangement and induce remarkable elastic deformation of constituent flakes under compression. During uncompression, the stress σ_x decreases quickly to the ambient pressure, and the energy dissipation during the loading-unloading process is indicated by the hysteresis loop of the stress-strain curve. Under tension, the stress increases almost linearly with the increasing loading strain ε_x when $\varepsilon_x < 0.3$, then keeps nearly an average constant with a little fluctuation induced by bond-breaking [18] in the range of $0.3 < \varepsilon_x < 0.66$. During the recovery process, the stress σ_x decreases quickly to the ambient zero pressure, and energy dissipation also happens, consistent with the compression-uncompression process. Despite of the bond breaking in GrF system at large tensile strain, the GrF nearly recovers to the initial state with a residual strain of 0.09. It is noted that only the response of GrFs under tension has been studied in previous work [18], the recovery process and the effect of bond-breaking on the recovery of GrFs have not been evaluated until now. Fig. 2a and b clearly show that the GrF exhibits good elastic deformation and recovery capability under both compression-uncompression and tension-untension processes. Furthermore, under the same loading strain amplitude, the GrF exhibits stronger recovery capability under compression than that under tension with a residual strain of 0.04 in the uncompression sample.

3.2. Three basic elastic deformation characteristics of GrFs

Based on the above simulation and the numerical model of 2D graphene, the total elastic deformation energy for each flake is calculated by $E^f_{elastic} = E^f_{bond} + E^f_{shear} + E^f_{bend}$, where $E^f_{elastic}$ is the total elastic energy for each flake, E^f_{bond}, E^f_{shear}, and E^f_{bend} are the elastic energies corresponding to the stretching, shearing and bending deformation of a flake, respectively. The distribution and evolution of $E^f_{elastic}$ for flakes in the system can be found in Fig. 3. Although the initial foam system (Fig. 3a) has been well equilibrated with the volume and the total energy converging to constants, see Fig. S1 in Supporting Information, we find that the elastic deformation of constituent flakes is much different from each other and the maximum elastic energy of flakes is of one order of magnitude larger than the minimum one indicated in the color bar in Fig. 3a. When the system is stretched continuously, the non-uniformity gets bigger and bigger as shown in Fig. 3b and c. When the tensile strain is up to 0.66 (Fig. 3c), the maximum deformation energy of flakes is nearly two orders of magnitude larger than the minimum one in the system. Furthermore, it is found that about 30% of the flakes in the system have about 70% of the total elastic energy of the whole system in the high-strain tension state as shown in Fig. 3c, which reflects highly non-uniform deformation at the scale of constituent flake in GrFs. It is also true in the uniaxial compression sample as shown in Fig. 3a, d and e. The bending, shearing and stretching deformation of constituent flakes were also observed in existing experiments

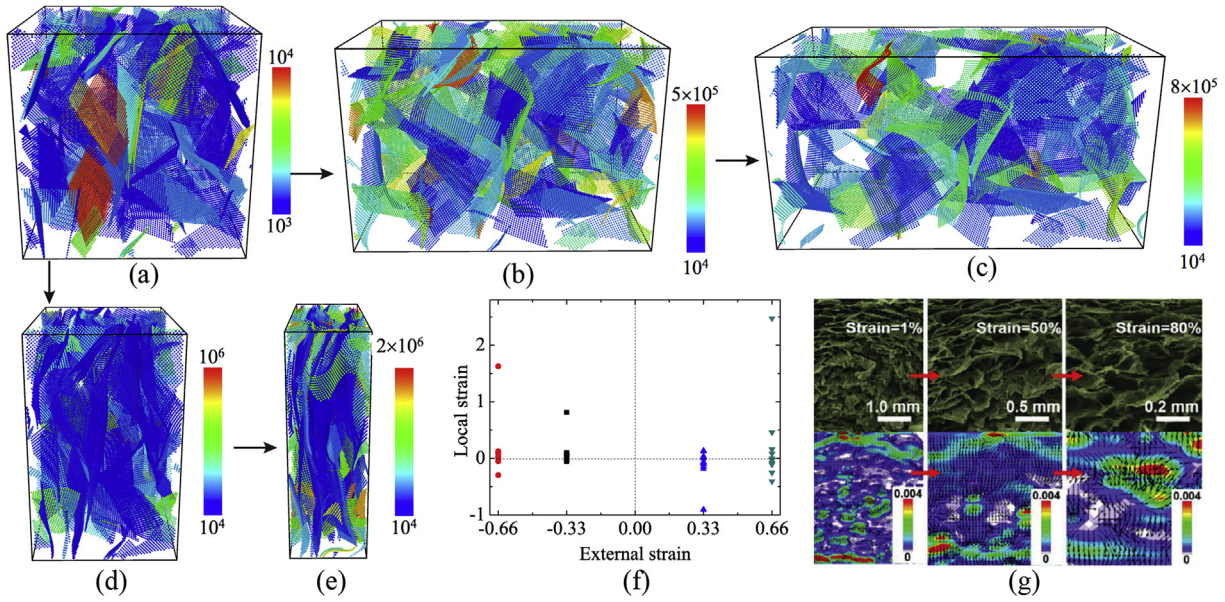

Fig. 3. The elastic deformation energy of each flake in the foam system under tension and compression. (a) The initial state; (b, c) The states with 0.33 and 0.66 tensile strain; (d, e) The states with 0.33 and 0.66 compressive strain. All flakes are colored according to their elastic deformation energy with the unit of energy Kcal/mol. (f) The local strain of ten pairs of beads as a function of the external loading strain ±0.33 and ± 0.66; (g) The structural evolution and strain map in a graphene foam material under compression [1], which were observed by *in situ* SEM. (A colour version of this figure can be viewed online.)

[11,32] and simulations [17,18,29], but such severe inhomogeneous deformation of flakes in GrFs has not been reported before. In addition, the deformation at a larger scale of local region is also non-uniform in graphene foams. To demonstrate this point, we randomly choose ten pairs of coarse beads from different flakes and find the local strain in the loading direction (x axis) when the external strain equals ±0.33 and ± 0.66, respectively. It is found that strains in ten local regions are much different from each other and also different from the externally macroscopic strain as shown in Fig. 3f, reflecting a highly non-uniform characteristic of GrF's deformation. Similar phenomenon was also observed experimentally as shown in Fig. 3g by Xu et al. [1] and Pranjal et al. [33] using *in situ* SEM. The characteristic of non-uniform deformation found in GrFs was also observed in their counterparts of fiber networks [34,35].

Furthermore, deformation energies E_{bond}, E_{shear} and E_{bend} as well as the adhesion energy between neighboring flakes E_{pair} in the whole system under tensile and compressive strains are examined as shown in Fig. 4a and b. Under tension, the stretching energy E_{bond} and the bending energy E_{bend} increase with the tensile strain and then keep nearly a constant when the strain is larger than a critical value ~0.3, while E_{pair} and E_{shear} have negligible increase during the whole tension process. Comparing the four energies finds that E_{bend} is the largest one and almost three times of E_{bond} in a broad loading strain range. This indicates that the elastic deformation of the foam system under tension is dominated by the bending deformation of flakes rather than the stretching one. Under compression as shown in Fig. 4b, the bending energy E_{bend} increases greatly and is obviously larger than the slightly increased E_{bond} and E_{shear}. The adhesion energy E_{pair} keeps nearly a constant when the compressive strain is smaller than 0.4, and then increases linearly with the compressive strain, reflecting that more local surface-surface structures produced due to massive flake rearrangements under further compression. To further demonstrate that it is the flake bending rather than stretching that dominates the elastic deformation under both tension and compression, we plot the ratio of E_{bend}/E_{bond} as a function of the tensile or compressive strain as shown in Fig. 4c. It is obvious that the ratio under both compression and tension loads is larger than 1. Under compression, the ratio increases from about 4 of the initial value to about 7 of the final value when the compressive strain is up to 0.65. Different from that under compression, with the tensile strain increasing, the ratio decreases first to about 2, and then increases with an abrupt transition at the critical strain p1, where the first local bond-breaking is detected and shown in Fig. 4c with a blue solid curve. Due to the breakage of crosslinks, the topology of the local region nearby changes greatly and up to 80% of the elastic energy in related flakes is released as shown in Fig. 4d, where the current elastic energy of each flake is labeled. In order to demonstrate that the bond-breaking should be responsible for the transition of the ratio E_{bend}/E_{bond} at the critical strain p1, we assume that all crosslinks and bonds in the system would not break. The simulation results show that the transition point would not appear any more, and the ratio decreases monotonically to something smaller than 1 when the tensile strain is up to p2 depicted as the dashed line in Fig. 4c. Actually, due to the inevitable breakage of C-C bond under tension in a realistic foam system, the fraction of broken bond will increase with the increasing tensile strain as shown by the blue solid curve in Fig. 4c. As a result, the ratio is always larger than 1, which indicates that the elastic deformation of GrFs under tension is always dominated by the flake bending rather than stretching, the same as that under compression. It should be noted that the finding of flake bending dominated mechanism holds not only for the present GrF system, but also for the system composed of flakes with intrinsic holes [19], or flakes of different sizes, shapes and thickness. Furthermore, this finding is also independent of the stiffness or density of crosslinks. Evidence can be found in Figs. S2 and S3 in Supporting Information. Such a mechanism is also unrelated to the size of the numerical sample as shown in Fig. S4 in Supporting Information, where a larger GrF system composed of 300 square coarse-grained graphene flakes with an equilibrated size of $338 \times 339 \times 329\ nm^3$ is adopted and the same mechanism is achieved.

It has been shown in Fig. 2a that the elastic recovery of GrFs

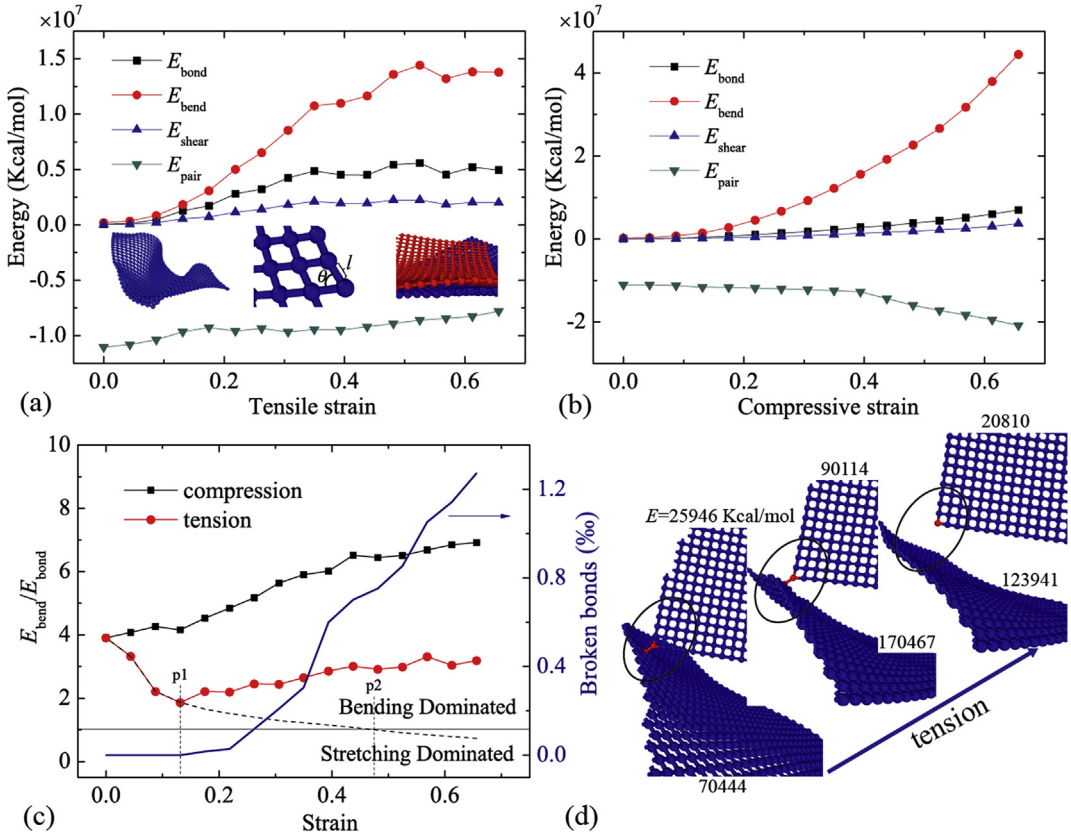

Fig. 4. The stretching energy (E_{bond}), the out-of-plane bending energy (E_{bend}), the in-plane shear energy (E_{shear}) and the van der Waals energy (E_{pair}) as a function of the strain in the graphene foam composed of 5-layered flakes under (a) the uniaxial tension and (b) the uniaxial compression; (c) The ratio E_{bend}/E_{bond} and fraction of broken bonds as a function of the compressive and tensile strain. (d) Variation of the local topology and elastic energy due to the breakage of local crosslinks. (A colour version of this figure can be viewed online.)

under tension and compression is different from each other, although the dominated modes of deformation under two types of loads are the same. To unveil the underlying mechanisms, we measured the ability of energy storage of GrFs by the elastic energy density $\rho_E = E_{elastic}/V$, in which V is the current volume of the system. The relationship of the elastic energy density ρ_E and the fraction of broken bonds as a function of the loading strain is given in Fig. 5a. For a better comparison, the absolute value of the tensile and compressive strains is used. The elastic energy density ρ_E under both compression and tension is nearly the same when the loading strain is smaller than 0.3, after that, it increases constantly under further compression while keeps nearly a constant under further tension. It can be explained by the difference of broken bond number in two systems: only a small number of bonds break when the compressive strain is larger than 0.6, while bond breaking under tension occurs as early as the system is stretched to the strain about 0.15, the number of which increases obviously under further tension. Broken bonds under the same tensile and compressive strains 0.66 are highlighted in red colors as shown in Fig. 5b and c, where few broken bonds can be found under compression as shown in Fig. 5b, but a large number of broken bonds are induced under tension as shown in Fig. 5c. Under tension, most of the broken bonds happen between flakes due to the tearing behavior as shown in the inset in Fig. 5c. The elastic energy of broken bonds will be dissipated completely and the elastic energy of flakes connected to the broken bonds will also be released partially during the flake rearrangement process as depicted in Fig. 4d. As a result, local regions near the broken bond would lose their elasticity to some extent and would severely impede recovery of the whole system during the subsequent recovery process. Under tension, there are many such regions in GrFs, which prevent recovery of the system, leading to larger residual strains as shown in Fig. 5d. By comparison, residual strains are much close under compression at different strain magnitudes as shown in Fig. 5e.

3.3. Factors influencing the elasticity of GrFs

Effects of the graphene flake size and thickness and the inter-flake crosslink density and stiffness on the elasticity of GrFs under both compression and tension are studied in this section. The effect of flake size and thickness on the elastic energy density of GrFs under tension and compression is shown in Fig. 6. Three foam systems composed of graphene flakes with the same thickness of 5-layered graphene sheets and the same crosslink number density of 6.9 per flake but different flake sizes of 75, 100 and 125 nm are used. As shown in Fig. 6a and b, the elastic energy density decreases with the increasing size of constituent flakes under both tension and compression, which is due to the different system densities. The equilibrium volume density of the graphene foam decreases from 200 mg/cm^3 to 72 mg/cm^3 when the size of flakes increases from 75 to 125 nm. Therefore, for a system containing larger flakes, fewer graphene flakes per unit volume are deformed during the loading process, which leads to a decreasing elastic energy density. In order to study the effect of flake thickness on the storage of elastic energy, we built four graphene foam systems with the same flake size of 75 nm and the crosslink number density 6.9 per flake, but different flake thickness of 1, 3, 5 and 7 layers. For the system with thinner flakes of 1, 3 and 5 layers, the elastic energy density increases with the flake thickness during both the compressive and tensile processes. Bonds and crosslinks break more easily under high loading

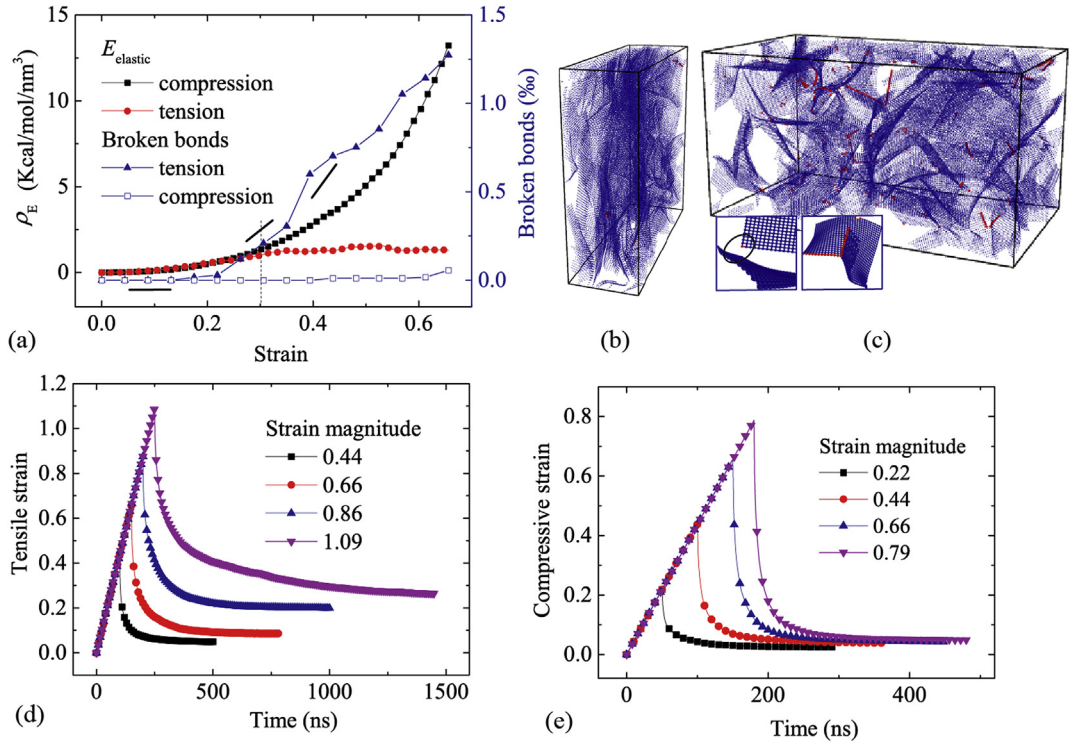

Fig. 5. (a) The elastic energy density and the fraction of broken bonds as a function of the compressive and tensile strains; (b, c) Distribution of broken bonds when the system is under the same tensile and compressive strains 0.66, respectively; The tensile and compressive strains as a function of the collapsed time under (d) tension-untension and (e) compression-uncompression. (A colour version of this figure can be viewed online.)

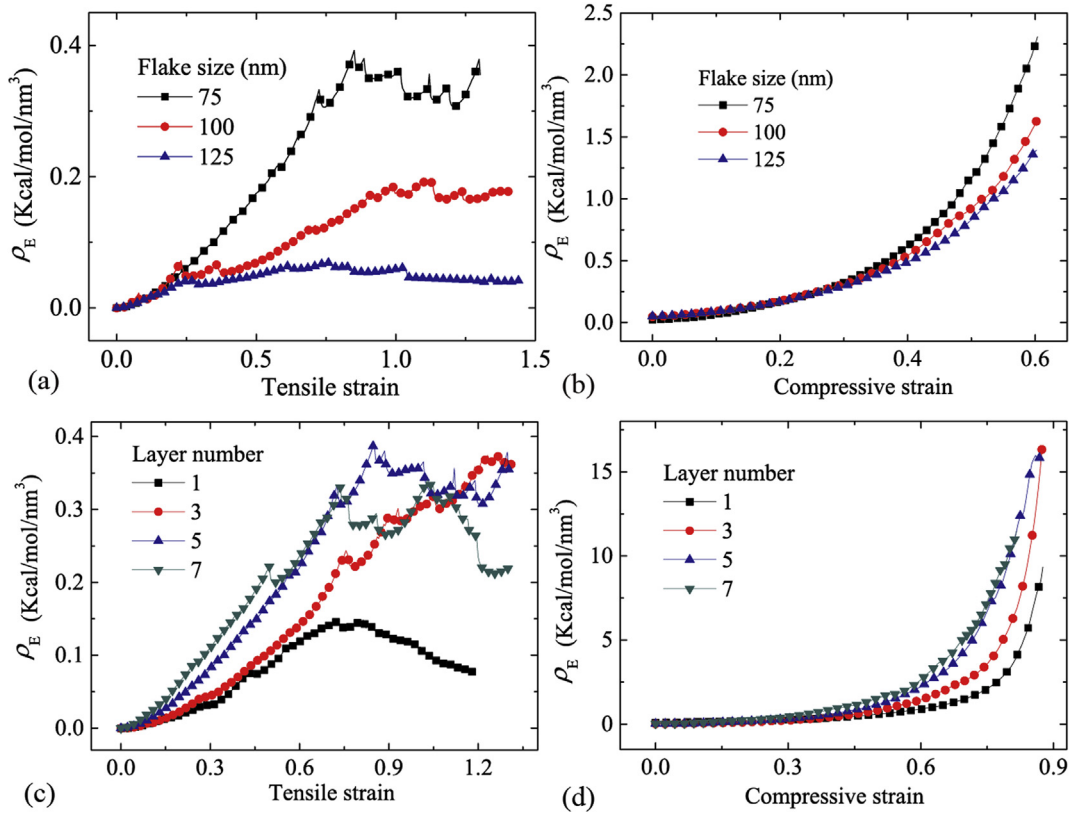

Fig. 6. The elastic energy density as a function of the uniaxially tensile strain and compressive strain in GrF systems with (a, b) flakes of different sizes and (c, d) flakes formed by different-layered graphene sheets. (A colour version of this figure can be viewed online.)

strain due to the relatively weak deformation coordination of thicker flakes. So, for the system with 7-layered thick flakes, the elastic energy density decreases drastically and becomes smaller than that of the system with thinner flakes when the system is stretched to the tensile strain of about 0.75.

Inter-flake crosslinks are used to link neighboring flakes to form a 3D interconnected network. The crosslink number density is tuned in a wide range of 0–27.5 per flake to study its effect on the storage of elastic energy of GrFs composed of 5-layered flakes with the side length of 75 nm. As shown in Fig. 7a and b, it is found that the elastic energy density is nearly zero if inter-flake crosslink does not exist in the system, while it increases drastically with the number of crosslinks under both tension and compression. For the system without or with a small number of crosslinks, the interaction between neighboring flakes is dominated by van der Waals forces between neighboring flakes, which is too weak to restrict flakes' rearrangements, and the work of external loads is mainly dissipated by the flake rippling, impacting and sliding as found in Ref. [21] rather than stored as elastic energies in flakes. Furthermore, the effect of crosslink stiffness k_c is also studied as shown in Fig. 7c and d. For a given fracture strain, the larger the stiffness of crosslinks, the higher the fracture strength would be in our simulations. It is found that the influence of crosslink stiffness on the elastic energy density is negligible when the loading strain is smaller than a critical value of about 0.45 under tension or about 0.6 under compression. Beyond the critical strain, the elastic energy density of GrFs increases as the crosslink stiffness increases.

For the foam system, the van der Waals adhesion between neighboring flakes acts as a resistance during the recovery process, while the elastic energy of flakes stored in the loading process provides a driving force. We use the ratio $E_{elastic}/E_{pair}$ to measure the recovery ability of the foam system under compression and tension as shown in Fig. 8. It is shown that the ratio larger than 1 in loading process only exists in the system with a larger crosslink density ρ_c and the flake thickness n_L. In Fig. 8b, the ratio in two cases of $\rho_c/n_L = 27.5/5$ and 13.8/5 is larger than 1.0 under both compression and tension. The foam with $\rho_c/n_L = 27.5/5$ shows the best elastic recovery with snapshots given in Fig. 2. The other systems exhibit relatively poor elastic recovery. So, in order to obtain a good elasticity of GrFs, a moderate flake thickness should be chosen, *e.g.*, 5 layered flakes. More importantly, enough crosslinks should be added in the system to ensure a good elasticity because the elasticity of GrFs seems to be much sensitive to the density of crosslinks. Considering that crosslinks can only be added between neighboring flakes, a maximum density of crosslinks exists, which could be utilized to tune the properties of GrFs. In short, it provides a direct evidence in Fig. 8 that both a larger crosslink density and thicker flakes are the requirements to enable GrFs a good elasticity. Without one, the other suffers. This is also qualitatively consistent with previous experimental speculations in Xu et al. [1] and Wu et al. [2].

4. Conclusions

Systematic CGMD simulations of compression-uncompression and tension-untension are conducted to study the elastic characteristic of GrFs. The excellent compressive elasticity of GrFs is reproduced as that found in a series of experiments [1–4,10], and certain tensile elasticity is also observed. According to the simulations, we found three basic characteristics of GrF elasticity: the first is that GrF deformation is highly non-uniform at the scale of both flakes and local regions, which is qualitatively consistent with the previous experimental observations; The second is that GrF deformation is dominated by the flake bending rather than stretching or shearing under both tension and compression, which is also independent of the numerical system setting, such as the

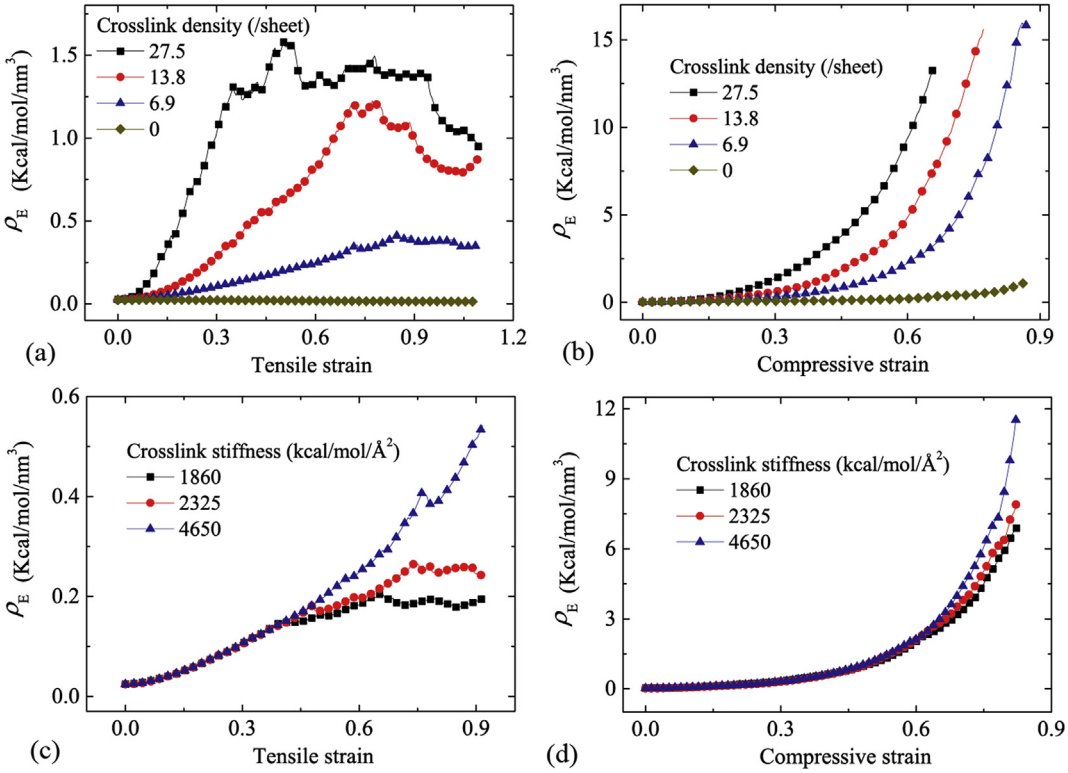

Fig. 7. The effect of the (a, b) crosslink density and (c, d) stiffness on the elastic energy density of graphene foams under both tension and compression. (A colour version of this figure can be viewed online.)

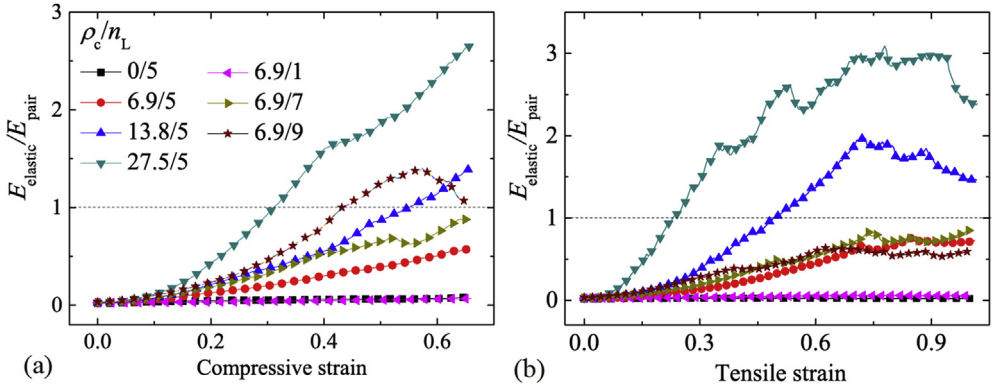

Fig. 8. The ratio of $E_{elastic}/E_{pair}$ as a function of (a) the compressive and (b) tensile strain for the system composed of 5-layered graphene flakes with crosslink density of 0, 6.9, 13.8 and 27.5 per flake, and for the system composed of 1-, 5-, 7- and 9-layered flakes with a fixed crosslink density of 6.9 per flake. (A colour version of this figure can be viewed online.)

size, shape or thickness of flakes, the density or stiffness of crosslinks; The third is that the asymmetry of elastic energy density under tension and compression is originated from the bond-breaking difference under the two loading conditions. Furthermore, effects of the size and thickness of flakes, and the density and stiffness of crosslinks on the elastic energy density of GrFs are investigated. It is found that the elastic energy density of GrFs decreases with the increasing flake size. A moderate thickness of flakes is good for the GrF elasticity. In addition, the elasticity is much sensitive to the crosslink density. The elastic energy density of the foam system increases greatly when more crosslinks are added. Stiffer crosslinks are benefit for promoting the elasticity of GrFs. Taking these factors into account yields that both thicker flakes and more crosslinks are two key factors responsible for a good elasticity of GrFs. Without one, the other suffers. The results in this paper should be very useful for understanding the elastic behavior of GrFs, and further design of advanced graphene-based materials.

5. Methods

The virial stress used in this paper is achieved according to the formula $\sigma_{xx} = \frac{1}{V}\sum_{\alpha}\left[\frac{1}{2}\sum_{\beta=1}^{N}(R_x^{\beta} - R_x^{\alpha})F_x^{\alpha\beta} + m^{\alpha}v_x^{\alpha}v_x^{\alpha}\right]$. Here, V is the total volume, R_x^{β} and R_x^{α} are positions of atoms α and β in the x axis. $F_x^{\alpha\beta}$ denotes the force acted on atom α due to atom β along the x axis. m^{α} and v_x^{α} are the mass of atom α and its velocity in the x direction, respectively. All simulations are implemented with an open source software Large-scale Atomic/Molecular Massively Parallel Simulator (LAMMPS) [36]. All figures and movies of the evolution of foam's structures are made using the open source software Ovito [37].

Author contributions

CW launched the project, carried out all simulations, and wrote the paper. SC supervised the study and revised the paper. All of the authors contributed to discussions.

Notes

The authors declare no competing financial interests.

Acknowledgements

CW acknowledges the support of NSFC through Grants #11602270, Strategic Priority Research Program of the Chinese Academy of Sciences (Grant No. XDB22040503). SC acknowledges the support of NSFC through Grants #11532013, #11872114. CZ acknowledges the support of NSFC Grants #11502150, the Natural Science Foundation of Hebei Province of China (A2016210060), and the Higher Education Youth Talents Program of Hebei Province of China (BJ2017052).

Appendix A. Supplementary data

Supplementary data to this article can be found online at https://doi.org/10.1016/j.carbon.2019.03.084.

References

[1] X. Xu, Q. Zhang, Y. Yu, W. Chen, H. Hu, H. Li, Naturally dried graphene aerogels with superelasticity and tunable Poisson's ratio, Adv. Mater. 28 (2016) 9223–9230.
[2] Y. Wu, N. Yi, L. Huang, T. Zhang, S. Fang, H. Chang, et al., Three-dimensionally bonded spongy graphene material with super compressive elasticity and near-zero Poisson's ratio, Nat. Commun. 6 (2015) 6141.
[3] L. Qiu, J.Z. Liu, S.L.Y. Chang, Y. Wu, D. Li, Biomimetic superelastic graphene-based cellular monoliths, Nat. Commun. 3 (2012) 1241.
[4] L. Qiu, B. Huang, Z. He, Y. Wang, Z. Tian, J.Z. Liu, et al., Extremely low density and super-compressible graphene cellular materials, Adv. Mater. 29 (36) (2017 Sep), 1701553.
[5] F. Yavari, Z. Chen, A.V. Thomas, W. Ren, H.-M. Cheng, N. Koratkar, High sensitivity gas detection using a macroscopic three-dimensional graphene foam network, Sci. Rep. 1 (2011) 1–5.
[6] S. Chen, P. Bao, X. Huang, B. Sun, G. Wang, Hierarchical 3d mesoporous silicon@graphene nanoarchitectures for lithium ion batteries with superior performance, Nano Res 7 (2014) 85–94.
[7] H. Bi, X. Xie, K. Yin, Y. Zhou, S. Wan, L. He, et al., Spongy graphene as a highly efficient and recyclable sorbent for oils and organic solvents, Adv. Funct. Mater. 22 (2012) 4421–4425.
[8] Z. Chen, W. Ren, L. Gao, B. Liu, S. Pei, H.-M. Cheng, Three-dimensional flexible and conductive interconnected graphene networks grown by chemical vapour deposition, Nat. Mater. 10 (2011) 424–428.
[9] Q. Peng, Y. Li, X. He, X. Gui, Y. Shang, C. Wang, et al., Graphene nanoribbon aerogels unzipped from carbon nanotube sponges, Adv. Mater. 26 (2014) 3241–3247.
[10] H. Hu, Z. Zhao, W. Wan, Y. Gogotsi, J. Qiu, Ultralight and highly compressible graphene aerogels, Adv. Mater. 25 (2013) 2219–2223.
[11] A. Nieto, B. Boesl, A. Agarwal, Multi-scale intrinsic deformation mechanisms of 3d graphene foam, Carbon 85 (2015) 299–308.
[12] C. Zhu, TY-j Han, E.B. Duoss, A.M. Golobic, J.D. Kuntz, C.M. Spadaccini, et al., Highly compressible 3d periodic graphene aerogel microlattices, Nat. Commun. 6 (2015) 1–8.
[13] Q. Zhang, F. Zhang, S.P. Medarametla, H. Li, C. Zhou, D. Lin, 3d printing of graphene aerogels, Small 12 (13) (2016 Apr 6) 1702–1708.
[14] Y. Xu, K. Sheng, C. Li, G. Shi, Self-assembled graphene hydrogel via a one-step hydrothermal process, ACS Nano 4 (2010) 4324–4330.
[15] M. Xu, D.N. Futaba, T. Yamada, M. Yumura, K. Hata, Carbon nanotubes with temperature-invariant viscoelasticity from -196 degrees to 1000 degrees c, Science 330 (6009) (2010 Dec 3) 1364–1368.
[16] J.A. Baimova, L.K. Rysaeva, B. Liu, S.V. Dmitriev, K. Zhou, From flat graphene to bulk carbon nanostructures, Phys. Status Solidi B 252 (7) (2015 Jul) 1502–1507.

[17] C. Wang, C. Zhang, S. Chen, The microscopic deformation mechanism of 3d graphene foam materials under uniaxial compression, Carbon 109 (2016) 666–672.
[18] D. Pan, C. Wang, T.C. Wang, Y. Yao, Graphene foam: uniaxial tension behavior and fracture mode based on a mesoscopic model, ACS Nano 11 (2017) 8988–8997.
[19] D. Pan, C. Wang, X. Wang, Graphene foam: hole-flake network for uniaxial supercompression and recovery behavior, ACS Nano 12 (11) (2018) 11491–11502.
[20] B. Boesl, The mechanics of energy dissipation in a three-dimensional graphene foam with macroporous architecture, Carbon 132 (2018) 59–64.
[21] C. Wang, D. Pan, S. Chen, Energy dissipative mechanism of graphene foam materials, Carbon 132 (2018) 641–650.
[22] N. Ni, S. Barg, E. Garcia-Tunon, F. MacUl Perez, M. Miranda, C. Lu, et al., Understanding mechanical response of elastomeric graphene networks, Sci. Rep. 5 (2015) 1–14.
[23] Z. Shen, H. Ye, C. Zhou, M. Kroeger, Y. Li, Size of graphene sheets determines the structural and mechanical properties of 3d graphene foams, Nanotechnology 29 (10) (2018 Mar 9), 104001.
[24] L. Ruiz, W. Xia, Z. Meng, S. Keten, A coarse-grained model for the mechanical behavior of multi-layer graphene, Carbon 82 (2015) 103–115.
[25] W. Xia, F. Vargas-Lara, S. Keten, J.F. Douglas, Structure and dynamics of a graphene melt, ACS Nano 12 (6) (2018 Jun 6) 5427–5435.
[26] F. Liu, C. Wang, Q. Tang, Conductivity maximum in 3d graphene foams, Small 14 (32) (2018), 1801458.
[27] Z. Qin, G.S. Jung, M.J. Kang, M.J. Buehler, The mechanics and design of a lightweight three-dimensional graphene assembly, Sci Adv 3 (1) (2017), e1601536.
[28] A.K. Geim, I.V. Grigorieva, Van der waals heterostructures, Nature 499 (2013) 419.
[29] S. Cranford, M.J. Buehler, Twisted and coiled ultralong multilayer graphene ribbons, Model. Simulat. Mater. Sci. Eng. 19 (2011), 054003.
[30] M. Dienwiebel, G.S. Verhoeven, N. Pradeep, J.W.M. Frenken, J.A. Heimberg, H.W. Zandbergen, Superlubricity of graphite, Phys. Rev. Lett. 92 (2004), 126101-1.
[31] C. Lee, X. Wei, J.W. Kysar, J. Hone, Measurement of the elastic properties and intrinsic strength of monolayer graphene, Science 321 (2008) 385–388.
[32] H. Sun, Z. Xu, C. Gao, Multifunctional, ultra-flyweight, synergistically assembled carbon aerogels, Adv. Mater. 25 (2013) 2554–2560.
[33] P. Nautiyal, M. Mujawar, B. Boesl, A. Agarwal, In-situ mechanics of 3d graphene foam based ultra-stiff and flexible metallic metamaterial, Carbon 137 (2018 Oct) 502–510.
[34] G.A. Buxton, N. Clarke, Bending to stretching" transition in disordered networks, Phys. Rev. Lett. 98 (23) (2007 Jun 8), 238103.
[35] D.A. Head, A.J. Levine, F.C. MacKintosh, Deformation of cross-linked semiflexible polymer networks, Phys. Rev. Lett. 91 (10) (2003 Sep 5), 108102.
[36] S. Plimpton, Fast parallel algorithms for short-range molecular dynamics, J. Comp. Physiol. 117 (1) (1995) 1–19.
[37] A. Stukowski, Visualization and analysis of atomistic simulation data with ovito–the open visualization tool, Model. Simulat. Mater. Sci. Eng. 18 (1) (2010), 015012-015019.